Int. J. Multiphase Flow, Vol. 3, pp. 445–457. Pergamon/Elsevier, 1977. Printed in Great Britain

LOCAL PROPERTIES OF VERTICAL MERCURY–ARGON TWO-PHASE FLOW IN A CIRCULAR TUBE UNDER TRANSVERSE MAGNETIC FIELD

I. MICHIYOSHI, H. FUNAKAWA, C. KURAMOTO, Y. AKITA and O. TAKAHASHI
Department of Nuclear Engineering, Kyoto University, Yoshida, Sakyo-ku, Kyoto, Japan

(*Received* 20 *June* 1976)

Abstract—Experimental data are presented in this paper on the profiles of local void fraction, bubble impaction rate, bubble velocity and its spectrum, and also bubble length and its spectrum, of mercury–argon two-phase slug flow flowing upwards in a vertical circular tube in the presence of a transverse magnetic field. Decrease in void fraction and increase in bubble velocity are significant when the magnetic flux density is larger than $0.3 \sim 0.4$ T($Ha \simeq 100$). This effect is discussed by analyzing the bubble size distribution. Recovery of local void fraction profile in the downstream of an obstacle and diffusion of void injected from only one nozzle in the presence of magnetic field are also discussed.

INTRODUCTION

Single phase flow of liquid metal in the presence of magnetic field has been studied theoretically and experimentally by many investigators. In this connection, an excellent review on the liquid metal magnetohydrodynamics(MHD) has been given and also the MHD problems in relation to the nuclear power including the cooling of blanket of nuclear fusion reactor have been discussed (Lielausis 1975). The effect of magnetic field, however, on two-phase flow of liquid metal has scarcely been analyzed except the experimental works of Thome (1964) and Fabris *et al.* (1975) for two-component two-phase flow. They have shown that the local void fraction is influenced by the presence of a magnetic field. In order to understand the characteristics of two-phase flow, we must first of all investigate experimentally the local properties such as the distribution of the gas and liquid phases, the bubble velocity and its spectrum, the bubble size distribution, the bubble impaction rate and so on.

This paper deals with the experimental data of the local properties mentioned above of mercury(liquid)–argon(gas) two-phase flow flowing upwards in a vertical circular tube under a transverse magnetic field. As will be mentioned later, the flow pattern in this study is slug flow. According to Baroczy's property index (1965, 1966),

$$Y = \left(\frac{\mu_L}{\mu_G}\right)^{0.2} \left(\frac{\rho_G}{\rho_L}\right) \qquad [1]$$

the present mercury–argon two-phase flow corresponds to a sodium (liquid and vapour) two-phase flow of $800 \sim 1000$°C.

EXPERIMENTAL FACILITY AND PROCEDURE

Experiments were carried out using the mercury loop of the Nuclear Power Experiment Facility in the Department of Nuclear Engineering, Kyoto University.

The experimental arrangement is shown schematically in figure 1. Distilled liquid mercury at room temperature is forced up by the diaphragm pump ⑧ from the lower tank ⑩ to the upper tank ⑨ where the liquid level is kept constant. From the upper tank it flows downwards and enters the mixing chamber ②, where the argon gas is injected through a series of 64 holes of 1 mm diameter spaced along the periphery of the 27.2 mm o.d. pipe merging into the mercury

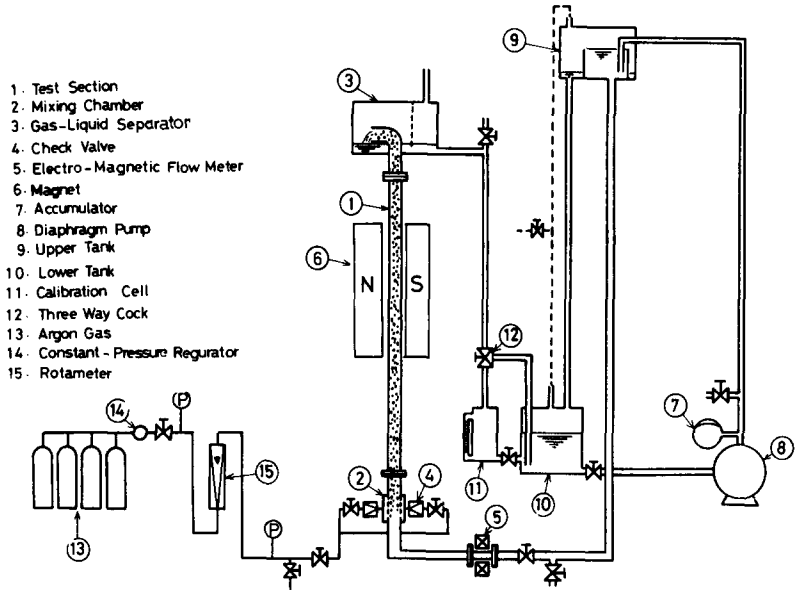

Figure 1. Experimental apparatus.

flow. The mercury–argon two-phase mixture flows upwards in a vertical circular lucite tube ① of $D = 2R = 20.2$ mm i.d. or SUS 304 stainless steel tube ① of $D = 2R = 23.0$ mm i.d. Subsequently, the argon gas is separated in the phase-separator ③, and only the mercury returns to the lower tank ⑩. The upper tank and the separator are 4 and 3 m above the ground respectively, and therefore there is a head difference of about 1 m to circulate the mercury. The flow rates of both fluids are measured by the electromagnetic flowmeter ⑤ and the rotameter ⑬, respectively.

The 2000 mm long vertical circular tube ① is placed at the 30 mm wide gap between the

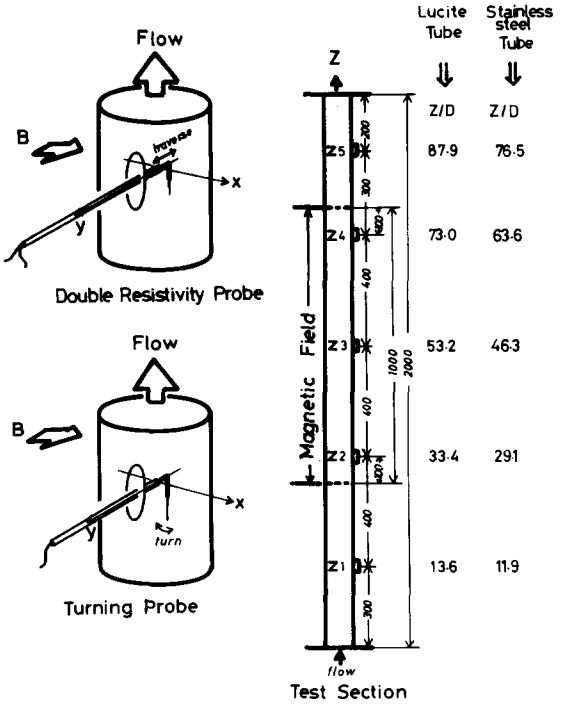

Figure 2. Important dimensions of test section.

magnetic pole pieces which are 50 mm wide and 1000 mm long, as shown in figure 2. The distribution of the magnetic flux is uniform, and its maximum density is 0.72 T.†

The local properties of two-phase flow at five positions Z_1 to Z_5 (figure 2) are measured by mainly using the same double-sensor probe (electrical resistivity probe) together with the same electronic equipment developed for the investigation of two-phase flow as shown in the paper of Serizawa *et al.* (1975*a*). The double-sensor probe is radially traversed in y-direction (perpendicular to the direction of the magnetic field) and it gives the distribution-data of local void fraction, bubble impaction rate, bubble velocity and its spectrum, bubble length (longitudinal) and its spectrum and so on. The distribution of local void fraction and bubble impaction rate in x-direction (parallel to the magnetic field) is measured by turning the single-sensor probe.

The ranges of the flow variables covered in this experimental study are: superficial mercury velocity $V_0 = 4Q_L/\pi D^2 = 0.39$–$0.79$ m/sec, its Reynolds number $Re = \rho_L V_0 D/\mu_L = 6.9 \times 10^4$ to 1.4×10^5, quality $X = W_G/(W_G + W_L) = 0.0043$–$0.0236\%$, Lockhart–Martinelli modulus $X_{tt} = (W_L/W_G)^{0.9}(\rho_G/\rho_L)^{0.5}(\mu_L/\mu_G)^{0.1} = 238.9$–$39.6$, volumetric flow rate ratio $\beta = Q_G/(Q_G + Q_L) = 0.112$–$0.543$, and Hartmann number calculated for liquid mercury $Ha = (DB/2)\sqrt{(\sigma_L/\mu_L)} = 34$–$219$.

The experiments were conducted mainly with the lucite tube.

EXPERIMENTAL RESULTS AND DISCUSSIONS

Typical profiles of local void fraction α_{loc} and bubble impaction rate N_b are shown in figures 3 and 4, respectively, where the axial position Z/D is taken as a parameter and only the position $Z/D = 87.9$ is out of magnetic field (figure 2). These profiles are almost symmetrical along the tube diameter and convex-shaped,‡ and they are similar to those of air–water two-phase slug flow (Serizawa *et al.* 1975*b*). The void fraction increases in z-direction by virtue of the pressure

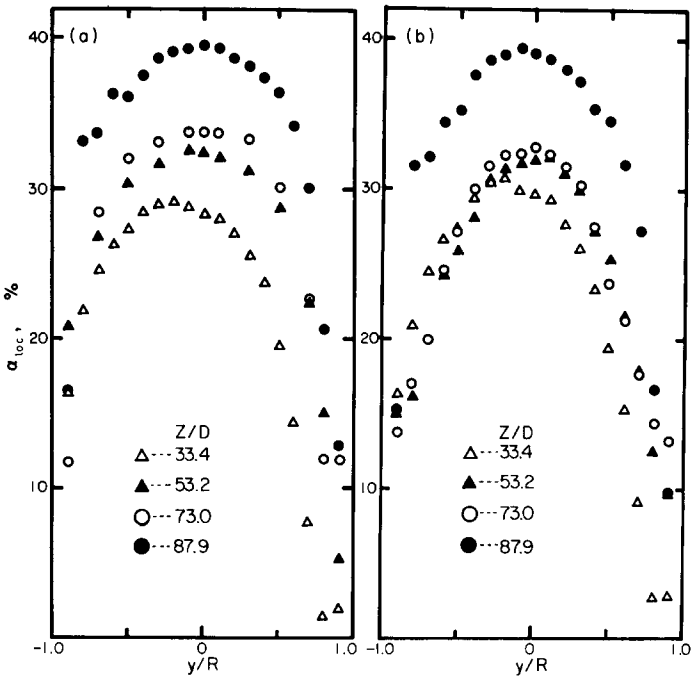

Figure 3a. Void fraction profile, lucite tube. $V_0 = 50$ cm/sec, $X = 0.0109\%$, $B = 0$ (T).

Figure 3b. Void fraction profile, lucite tube. $V_0 = 50$ cm/sec, $X = 0.0109\%$, $B = 0.57$ (T).

†T means tesla.

‡Convex-shaped profiles seem to be typical for slug flow of any liquid. Effects of non-wettability between mercury and the tube wall on the α_{loc} profiles have been discussed by Serizawa & Michiyoshi (1973).

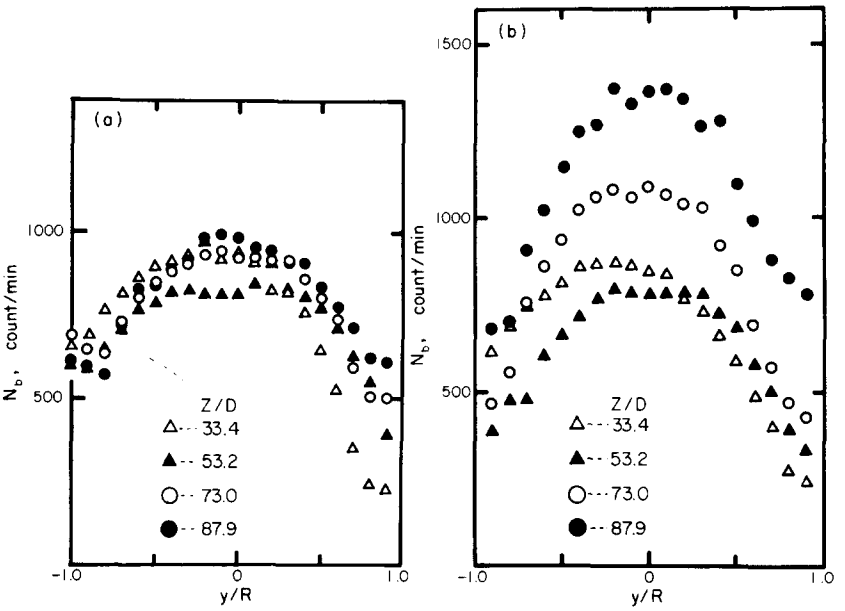

Figure 4a. Impaction rate profile, lucite tube. $V_0 = 50$ cm/sec, $X = 0.0109\%$, $B = 0$ (T).

Figure 4b. Impaction rate profile, lucite tube. $V_0 = 50$ cm/sec, $X = 0.0109\%$, $B = 0.57$ (T).

drop (figure 3a), while the bubble impaction rate does not change so much (figure 4a), in the case of $B = 0$. On the other hand, in the case of $B \neq 0$, an increase in bubble impaction rate can be seen (figure 4b), but a change in void fraction can be recognized only at $Z/D = 87.9$ (figure 3b). Therefore, most data are indicated at the position $Z/D = 73.0$ for the comparison between the two cases.

The effects of magnetic field on the profiles of local void fraction are shown in figure 5 (in x-direction) and figure 6 (in y-direction). Both profiles in x- and y-directions are almost

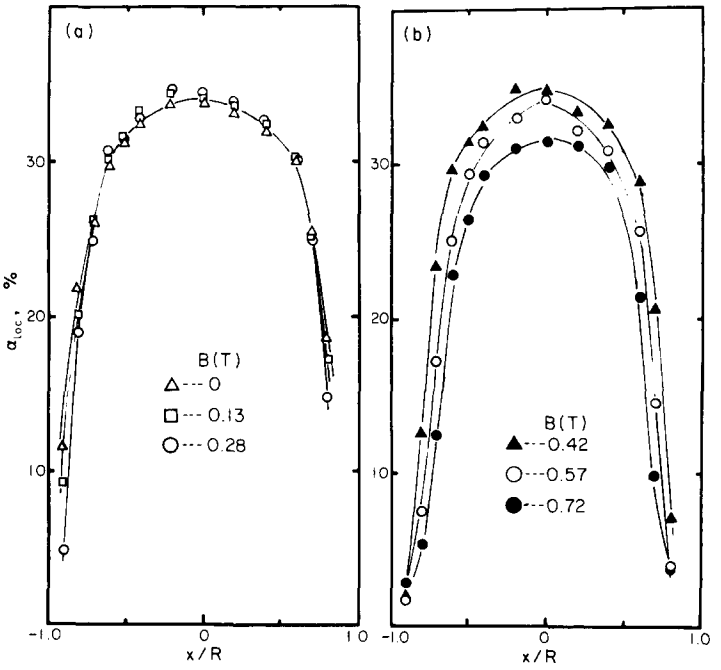

Figure 5a. Void fraction profile, lucite tube. $V_0 = 79$ cm/sec, $X = 0.0105\%$, $Z/D = 73.0$.

Figure 5b. Void fraction profile, lucite tube. $V_0 = 79$ cm/sec, $X = 0.0105\%$, $Z/D = 73.0$

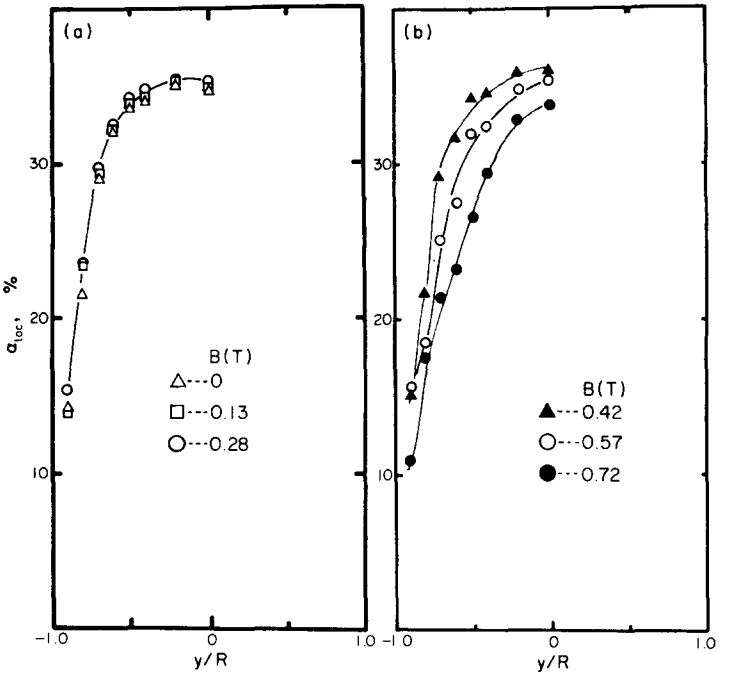

Figure 6a. Void fraction profile, lucite tube. $V_0 = 79$ cm/sec, $X = 0.0105\%$, $Z/D = 73.0$

Figure 6b. Void fraction profile, lucite tube. $V_0 = 79$ cm/sec, $X = 0.0105\%$, $Z/D = 73.0$.

identical, and a decrease in void fraction, as a whole, is remarkable when the magnetic flux density is larger than $0.3 \sim 0.4$ T.

The profiles of local void fraction obtained with the stainless steel tube (conducting wall) instead of the lucite tube (non-conducting wall) are shown in figure 7. As compared with figure 6, we can see similar profiles of α_{loc} and the same tendencies of the effect of magnetic field. Thome's (1964) data for NaK–N_2 two-phase flow through a stainless steel rectangular channel also show a decrease in void fraction and similar profiles of α_{loc} to those in figure 7 in the presence of a transverse magnetic field. At present, however, it is difficult to derive quantitatively the influence of wall conductance on the two-phase flow under the magnetic field.

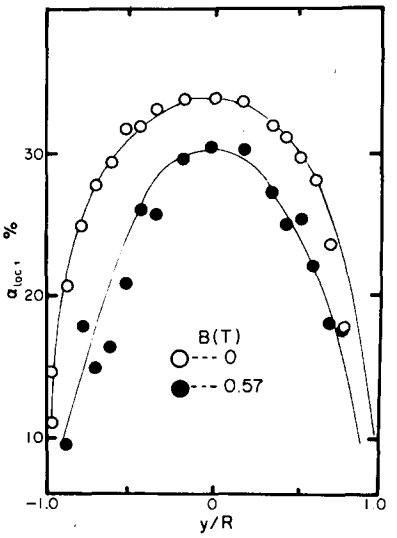

Figure 7. Void fraction profile, stainless steel tube. $V_0 = 39$ cm/sec, $X = 0.0117\%$, $Z/D = 63.6$.

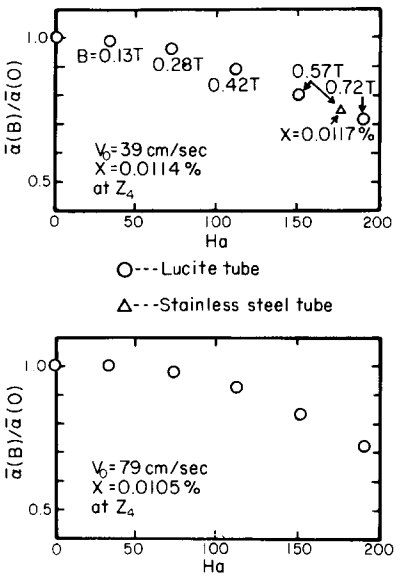

Figure 8. Average void fraction correlated with Hartmann number.

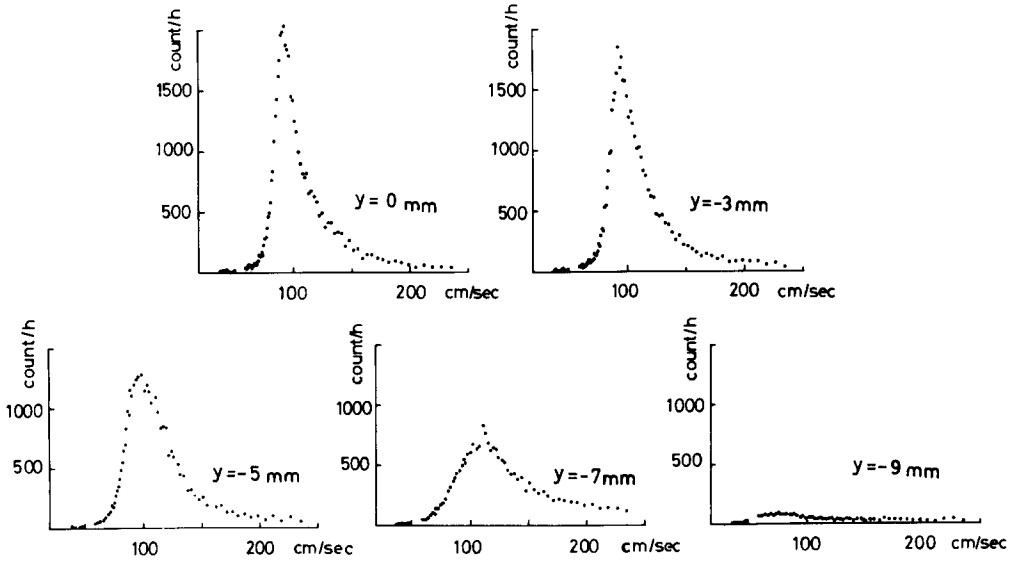

Figure 9a. Bubble velocity spectrum, lucite tube. $Z/D = 73.0$, $V_0 = 50$ cm/sec, $X = 0.011\%$, $B = 0$ (T).

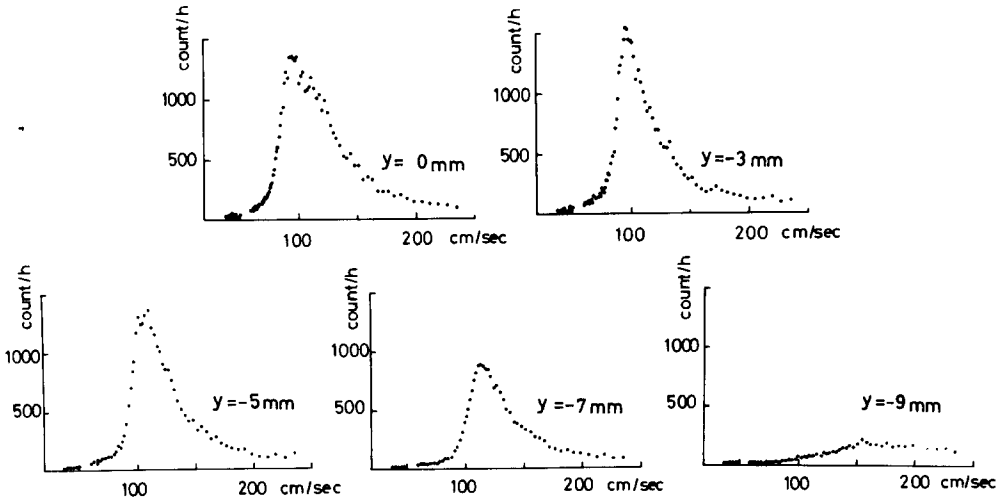

Figure 9b. Bubble velocity spectrum, lucite tube. $Z/D = 73.0$, $V_0 = 50$ cm/sec, $X = 0.011\%$, $B = 0.57$ (T).

The decrease in average cross-sectional void fraction $\bar{\alpha}$ at the position Z_4 with increasing the Hartmann number Ha calculated for liquid mercury is shown in figure 8. The datum for stainless steel tube is not different from that for lucite tube.

In order to understand the effect of magnetic field, we had to investigate the bubble velocity and bubble size distribution. Figures 9a ($B = 0$) and 9b ($B = 0.57$ T) indicate the bubble velocity spectrum obtained by the double-sensor probe together with a multichannel pulse height analyzer (see Serizawa *et al.* 1975*a*). From these figures, it can be seen that the sharp peak of the spectrum obtained near the axis of test tube becomes blunt and larger velocities are predominant when the magnetic field is applied. The average velocity V_b of the bubbles measured by the cross-correlation technique (see Serizawa *et al.* 1975*a*), as illustrated in figure 10, increases when B is larger than $0.3 \sim 0.4$ T and its increase is significant at $|y|/R = 0.5 \sim 0.6$. When B exceeds 0.4 T, the bubble velocity profile becomes M-shaped.

A comparison between figures 6 and 10 implies that the slip ratio V_G/V_L (ratio of gas to liquid phase velocity) increases and hence the void fraction decreases when the magnetic field is present, according to the equation

$$\frac{V_G}{V_L} = \frac{X}{1-X}\,\frac{1-\alpha}{\alpha}\,\frac{\rho_L}{\rho_G} \qquad [2]$$

at a fixed value of the quality X, as has been already pointed out by Thome (1964).

When the signals from the double-sensor probe are recorded on the linear recorder, we can obtain much more information by analyzing those graphic records. The histograms of bubble length (longitudinal) L_b detected at the radial positions $y/R = 0$, -0.3, -0.6 and -0.9 are indicated in figure 11, where "bubbles" and "slugs" are defined as $L_b < D$ (tube inside diameter) and $L_b > D$, respectively. The fact that "bubbles" are distributed independently of "slugs" indicates that the flow pattern in this study is slug flow and there exist "bubbles" in the wake of "slugs". Generally speaking, the count number decreases with increasing L_b. In the case of $B = 0$, there are comparatively more "bubbles" and no "slugs" near the tube wall ($y/R = -0.9$): while the number of "bubbles" increases and that of "slugs" decreases except at the tube wall, but "slugs" appear near the tube wall and "slugs" become longer on the average except at the tube axis, when $B = 0.57$ T is applied. Observation of the motion of bubbles

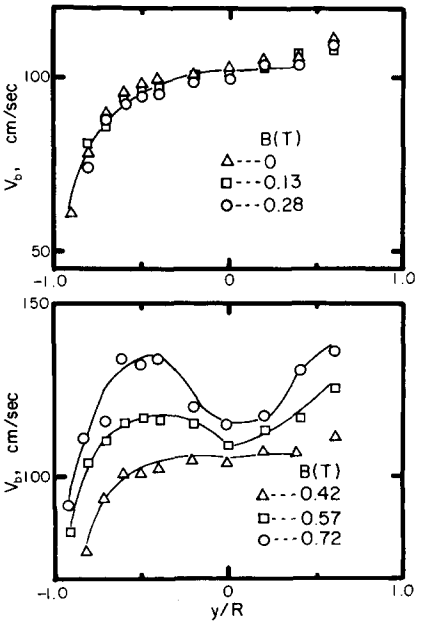

Figure 10. Bubble velocity profile, lucite tube. $Z/D = 73.0$, $V_0 = 57$ cm/sec, $X = 0.0106\%$.

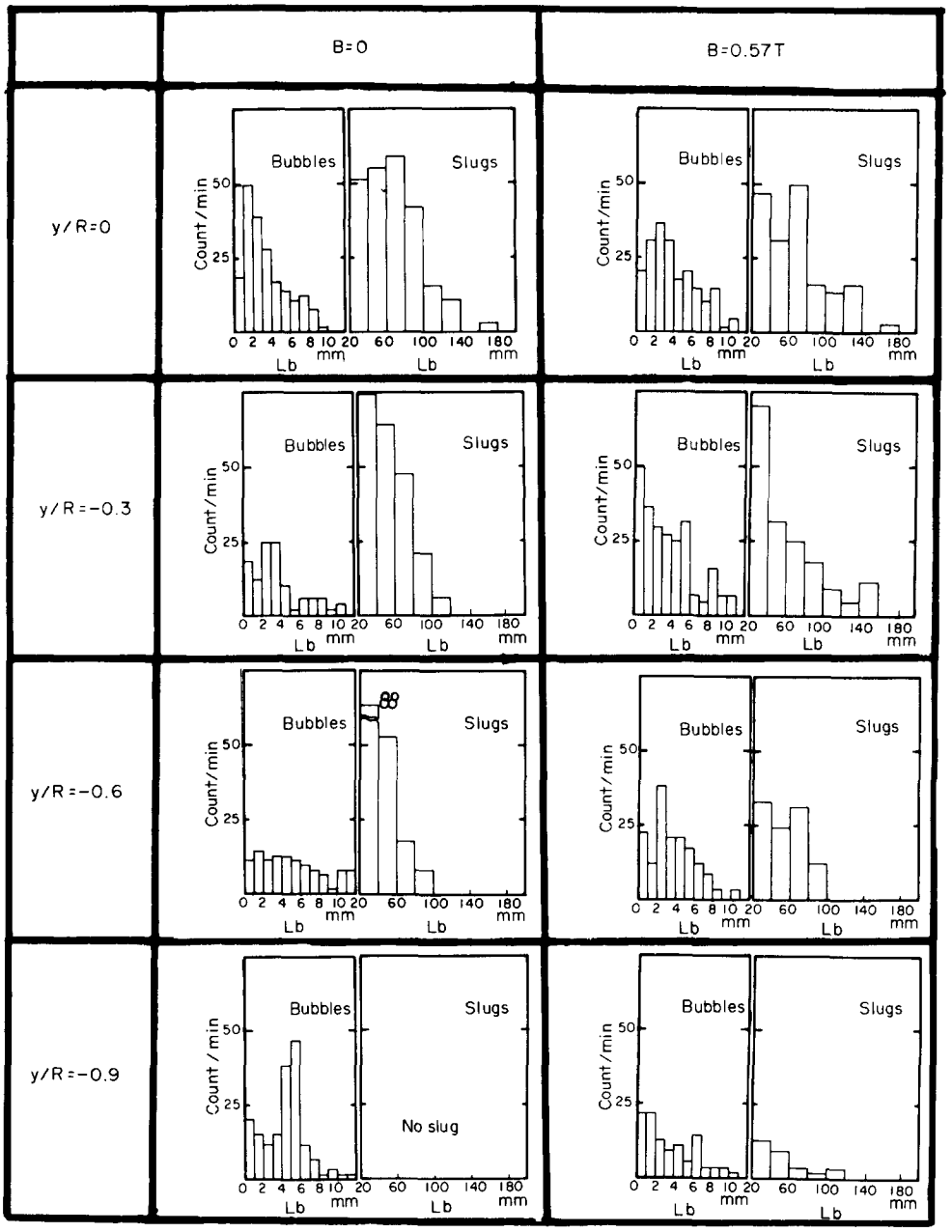

Figure 11. Bubble length histograms, lucite tube. $Z/D = 73.0$, $V_0 = 39$ cm/sec, $X = 0.0114\%$.

through the lucite tube wall confirms the characteristics shown in the histogram for $y/R = -0.9$. It should be noted that the number of signals from which the bubble length can not be calculated increases when the magnetic field is present. This may be due to the deformation of "slugs" and the irregular motion of "bubbles".

Figure 12 indicates the histograms of the velocity of "bubbles" and "slugs", which are of similar shape. The presence of magnetic field flattens the shape of both histograms and causes an increase in the velocity of "bubbles" and "slugs". The summation of "bubbles"—and "slugs"—histograms corresponds to the bubble velocity spectrum already shown in figure 9.

The contribution of the bubbles having various lengths to the local void fraction is shown in figure 13. From this figure, it can be seen that the "slugs" of $L_b > 20$ mm mainly contribute to the local void fraction. The combination of figures 10–13 indicates that a decrease in the number

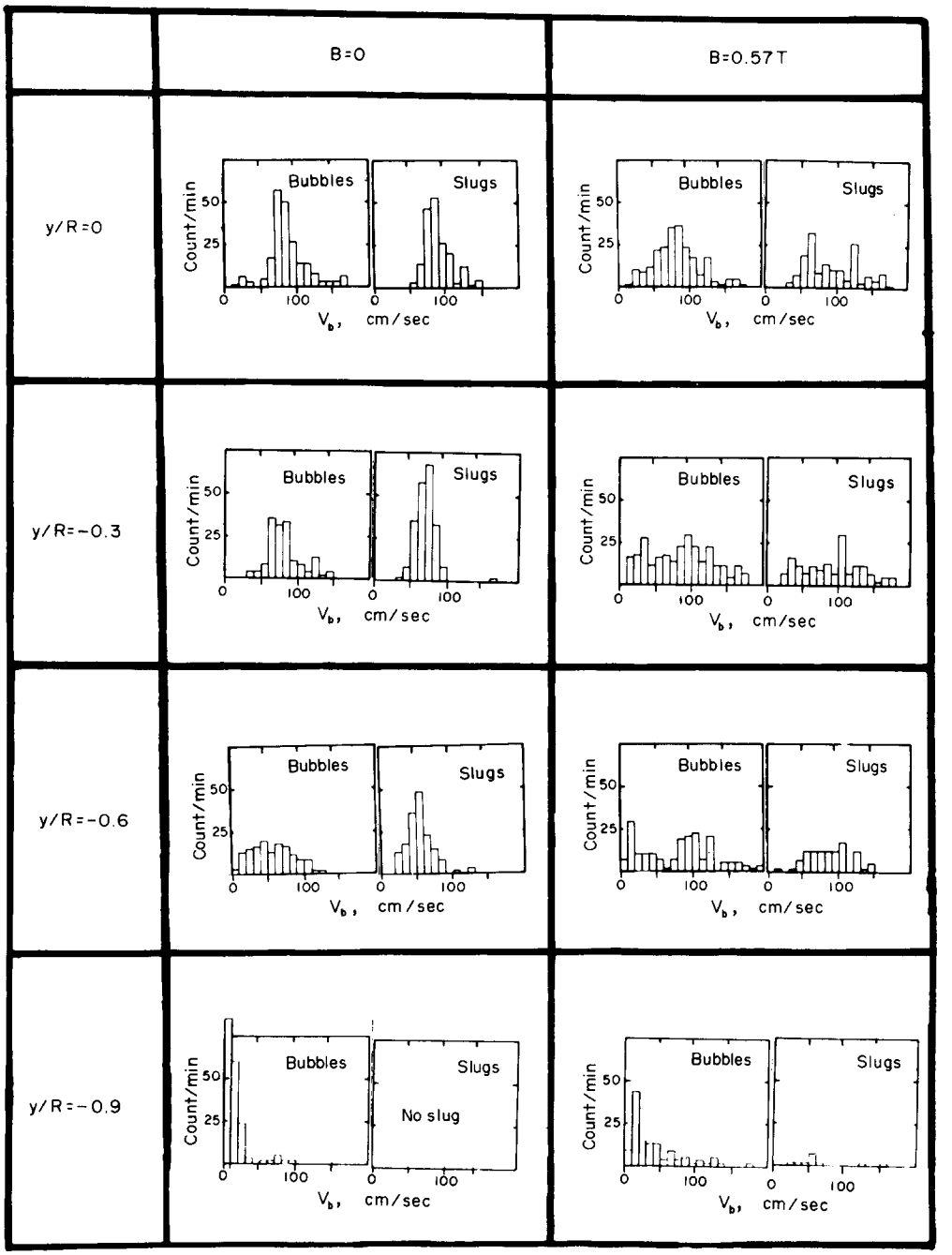

Figure 12. Bubble velocity histograms, lucite tube. $Z/D = 73.0$, $V_0 = 39$ cm/sec, $X = 0.0114\%$.

of "slugs" and an increase in their velocity mainly cause a decrease in the local void fraction in the presence of a magnetic field.

Lorentz force acts on the liquid metal. Deformed and elongated "slugs" can move easily because of their lower resistance.† "Bubbles" also can move easily in the wake of a high speed "slug". This seems to be the reason for the increase in the velocity of "bubbles" and "slugs". In this connection, a theoretical analysis remains in future study.

†Effect of bubble size and shape on the rise velocity of a single bubble in still liquid mercury was investigated by Hijikata *et al.* (1976). However, their data can not be applied directly to the two-phase flow which contains many bubbles by virtue of interaction between the bubbles.

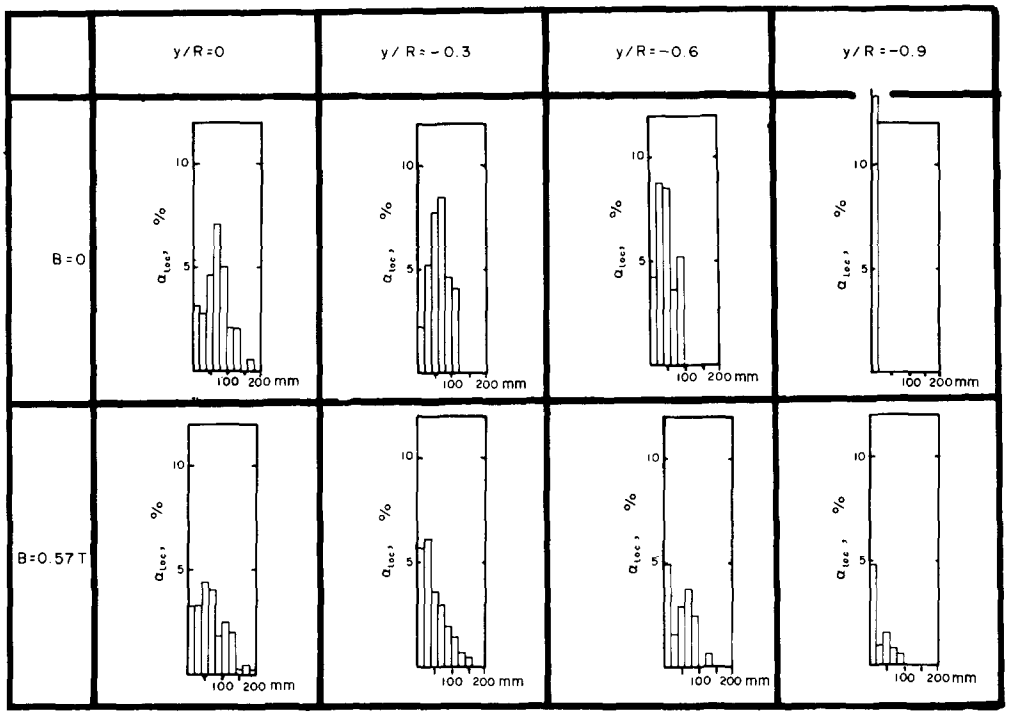

Figure 13. Bubble-contribution to void fraction, lucite tube. $Z/D = 73.0$, $V_0 = 39$ cm/sec, $X = 0.0114\%$.

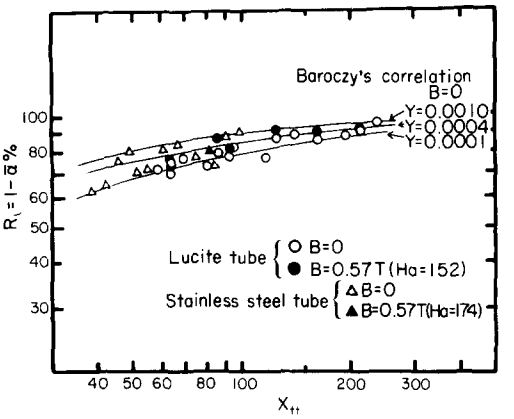

Figure 14. Average liquid fraction correlated with Lockhart-Martinelli modulus.

All data of average cross-sectional liquid fraction $R_L = 1 - \bar{\alpha}$ in the present study are correlated with Lockhart–Martinelli modulus X_{tt} in figure 14. Since the values of Baroczy's property index Y are 0.0004–0.0008 in the present experiments, the data, as a whole, are a little below the Baroczy's correlation curve in the case of $B = 0$.‖ As already mentioned in figure 8, the liquid fraction R_L increases with increasing the magnetic flux density.

It is very important to investigate the behavior of two-phase flow in the downstream of an obstacle when the magnetic field is present. At the position Z_2 (see figure 2) an obstacle of rectangular shape is introduced, having the dimensions of 5×10 mm and 2 mm thickness. The profiles of local void fraction measured at Z_3, Z_4 and Z_5 in the presence of the obstacle close to the tube wall on the y axis at Z_2 are shown in figure 15. With no magnetic field present, the profile has already recovered and is symmetric again at Z_3. In the presence of a magnetic field,

‖Discussions about the Baroczy's correlation for liquid metal two-phase flow have been presented by Serizawa & Michiyoshi (1973).

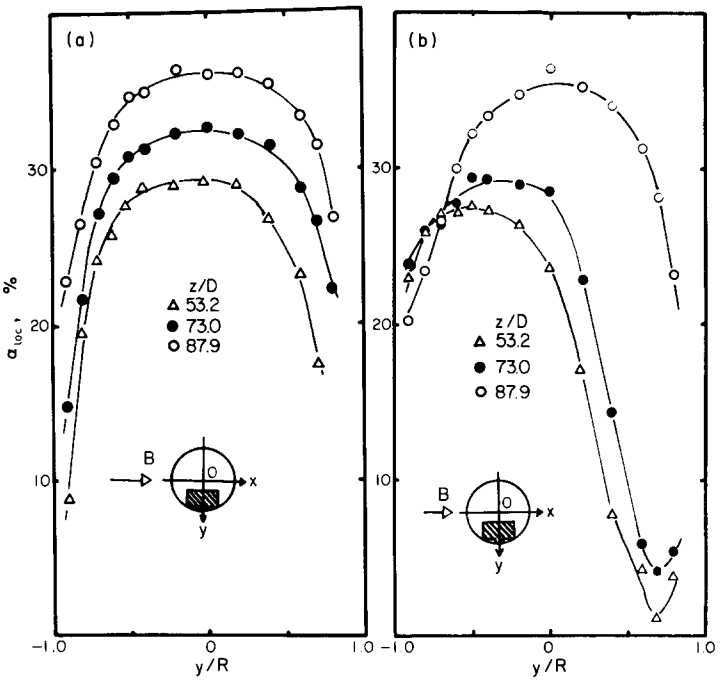

Figure 15a. Void fraction profile in the downstream of an obstacle, lucite tube. $V_0 = 39$ cm/sec, $X = 0.0114\%$, $B = 0$ (T).

Figure 15b. Void fraction profile in the downstream of an obstacle, lucite tube. $V_0 = 39$ cm/sec, $X = 0.0114\%$, $B = 0.57$ (T).

the recovery of the void fraction profile is very slow as can be seen from the profiles at Z_3 and Z_4, and a symmetric profile is established only at Z_5 (outside of magnetic field). Figure 16 shows the local void fraction map at Z_4. It can be seen that the void is apt to move to the opposite side of the obstacle in y-direction (perpendicular to the magnetic field direction), but not in x-direction (parallel to the magnetic field). These effects can also be confirmed by introducing the obstacle close to the tube wall on the x axis at Z_2, as shown in figure 17. It shows a symmetric profile of the local void fraction at Z_4 even in the presence of the magnetic field.

The profiles of the local void fraction measured at Z_4, when the argon gas is injected from only one nozzle of 2 mm i.d. close to the tube wall at Z_2 (we did not use the mixing chamber in this case), are shown in figure 18. Since the maldistribution of void is significant on the y axis in the presence of the magnetic field, we gain the information that the diffusion of void is retarded in the magnetic field.

From figures 15 to 18, it should be noted that we have to pay attention to the maldistribution of void in the presence of a magnetic field when the liquid metal two-phase flow is applied to the nuclear power facility.

CONCLUSIONS

A considerable amount of information has been obtained on the local properties of mercury–argon two-phase slug flow flowing upwards in a vertical circular tube in the presence of a transverse magnetic field. Comparing the data with experiments with no magnetic field present, and correlating the average void and liquid fractions with Hartmann number and Lockhart–Martinelli modulus, the effects of magnetic field on the two-phase flow are summarized as follows:

(1) The local void fraction profiles of convex shape in x- and y-directions are almost identical. A decrease in void fraction and an increase in bubble velocity are significant when the

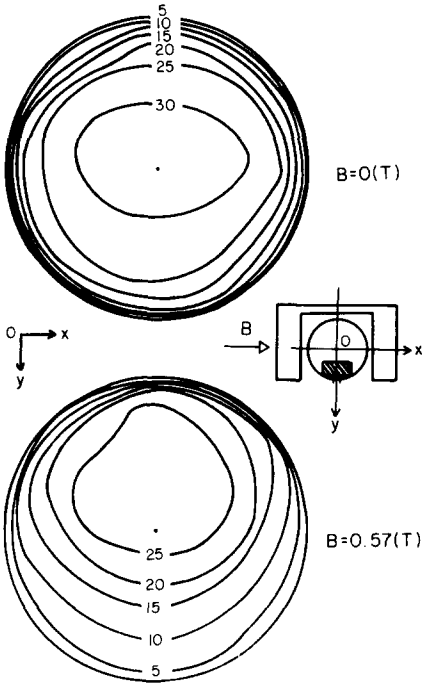

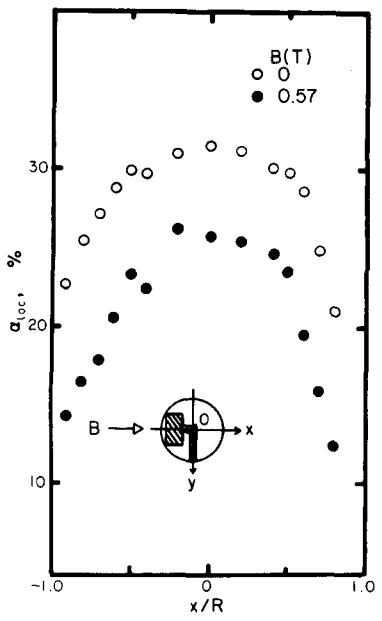

Figure 16. Void fraction map in the downstream of an obstacle, lucite tube. $V_0 = 39$ cm/sec, $X = 0.0114\%$, $Z/D = 73.0$.

Figure 17. Void fraction profile in the downstream of an obstacle, lucite tube. $V_0 = 39$ cm/sec, $X = 0.0114\%$, $Z/D = 73.0$.

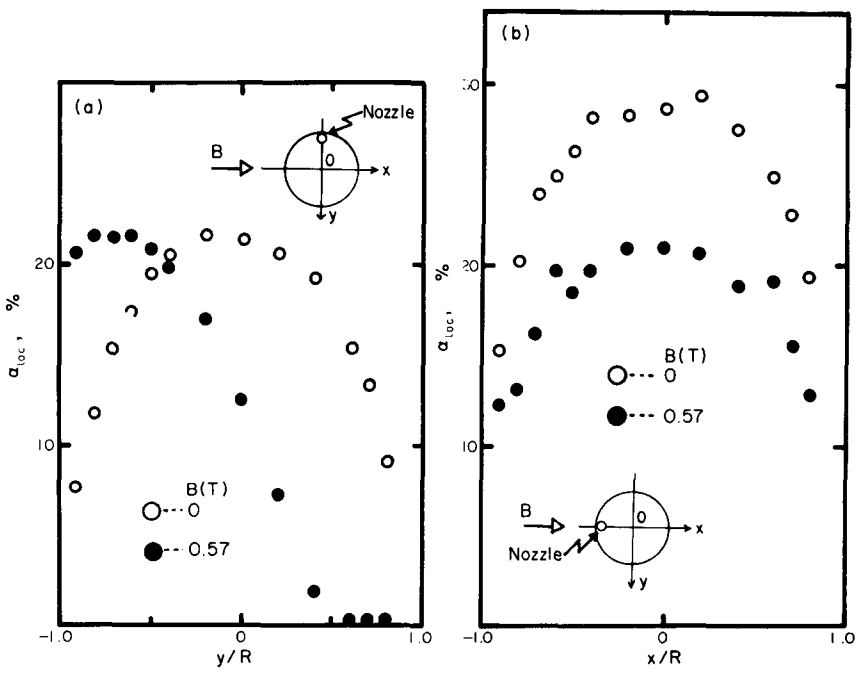

Figure 18a. Void fraction profile in the downstream of gas-injection from one nozzle, lucite tube. $Z/D = 73.0$, $V_0 = 39$ cm/sec.

Figure 18b. Void fraction profile in the downstream of gas-injection from one nozzle, lucite tube. $Z/D = 73.0$, $V_0 = 39$ cm/sec.

magnetic flux density is larger than $0.3 \sim 0.4$ T ($Ha \simeq 100$). The bubble velocity profile becomes M-shaped.

(2) Bubble velocity spectrum becomes flat and larger velocities are predominant.

(3) The number of "bubbles" increases and that of "slugs" decreases except at the tube wall, but "slugs" appear near the tube wall and "slugs" become longer on the average except at the tube axis.

(4) Decrease in the number of "slugs" and increase in their velocity mainly cause a decrease in local void fraction.

(5) Recovery of the local void fraction profile in the downstream of an obstacle and the diffusion of void injected from only one nozzle are retarded in y-direction.

It should be noted that we have to pay attention to these phenomena in relation to the nuclear power.

REFERENCES

BAROCZY, C. J. 1965 Correlation of liquid fraction in two-phase flow with application to liquid metals. *Chem. Engng Progr. Symp. Ser.* **61**, 179.

BAROCZY, C. J. 1966 Comparison of two-phase liquid fraction data for potassium with other fluids. *A.I.Ch.E. Jl* **12**, 1028–1029.

FABRIS, G., COLE, R. L. & HANTMAN, R. G. 1975 Fluid dynamic studies of two-phase liquid–metal flow in an MHD generator. *Proc. 6th Int. Conf. on MHD.* **3**, 363–376.

HIJIKATA, K., MORI, Y. & WATABE, S. 1976 Bubble dynamics in mercury. *Trans. Jap. Soc. Mech. Engrs* **42**, 2133–2140.

LIELAUSIS, O. 1975 Liquid–metal magnetohydrodynamics. *Atomic Energy Rev.* **13**, 527–581.

SERIZAWA, A., KATAOKA, I. & MICHIYOSHI, I. 1975*a* Turbulence structure of air–water bubbly flow—I. Measuring techniques. *Int. J. Multiphase Flow* **2**, 221–233.

SERIZAWA, A., KATAOKA, I. & MICHIYOSHI, I. 1975*b* Turbulence structure of air–water bubbly flow—II. Local properties. *Int. J. Multiphase Flow* **2**, 235–246.

SERIZAWA, A. & MICHIYOSHI, I. 1973 Void fraction and pressure drop in liquid metal two-phase flow. *J. Nucl. Sci. Technol.* **10**, 435–445.

THOME, R. J. 1964 Effect of a transverse magnetic field on vertical two-phase flow through a rectangular channel. ANL-6854.